

Anomalous Soft Dynamics of Water in a Nanotube: A Revelation of Nanoscale Confinement

Alexander I. Kolesnikov, Jean-Marc Zanotti,* Chun-Keung Loong, and Pappannan Thiagarajan
Intense Pulsed Neutron Source Division, Argonne National Laboratory, Argonne, Illinois 60439, USA

Alexander P. Moravsky and Raouf O. Loutfy
MER Corporation, 7960 South Kolb Road, Tucson, Arizona 85706, USA

Christian J. Burnham
University of Utah, Salt Lake City, Utah 84112, USA
(Received 23 December 2003; published 14 July 2004)

Quasi-one-dimensional water encapsulated inside single-walled carbon nanotubes, here referred to as *nanotube water*, was studied by neutron scattering. The results reveal an anomalously soft dynamics characterized by pliable hydrogen bonds, anharmonic intermolecular potentials, and large-amplitude motions in nanotube water. Molecular dynamics simulations consistently describe the observed phenomena and propose the structure of nanotube water, which comprises a square-ice sheet wrapped into a cylinder inside the carbon nanotube and interior molecules in a chainlike configuration.

DOI: 10.1103/PhysRevLett.93.035503

PACS numbers: 63.22.+m, 61.12.-q, 61.46.+w

Water confined in nanoscale one-dimensional channels is of great interest to biology, geology, and materials science. An excellent model for such a system is water in single-walled carbon nanotubes (SWNT) [1,2], realized by the unique geometry of nanotubes and the weak interaction between the water molecules and carbon atoms. As a result of nanoscale confinement, the physical properties of this quasi-one-dimensional water, referred to as nanotube water, are expected to differ from those of the bulk counterparts. A joint neutron-scattering and molecular-dynamics (MD) study combines the advantages of the extraordinarily large neutron scattering cross section of hydrogen and the rigorous comparison of the experimental data with the simulations. Neutron diffraction (ND) and inelastic neutron scattering (INS) over a wide range of momentum and energy transfers were performed to characterize the structure and dynamics of nanotube water/ice. Among the previous MD simulations of water plus nanotubes (see, for example, Refs. [3–9]), Martí and Gordillo [10,11] and Mann and Halls [12] calculated the vibrational bands and diffusive behavior of water in SWNT, which provided useful insight into the present investigation. Our MD simulations were based on a rigid SWNT of length 40 Å that interacts with water molecules through a previously established Lennard-Jones (LJ) potential [13]. The TTM2-F polarizable flexible water model employed here was shown to successfully account for the electronic structure data of small water clusters and to reproduce the bulk properties of ice and ambient liquid water [14,15]. The Ewald sum for the long-range Coulomb interactions and standard boundary conditions were used.

We first examined by ND the entry and encapsulation of water in open-ended SWNT of $\sim 14 \pm 1$ Å diameter and ~ 10 nm average length. A high-quality SWNT sample (3.8 g) was prepared using a method described

elsewhere [16]. The high purity and the narrow variation of the nanotube diameter were quantified by transmission electron microscopy and Raman measurements. To fill the SWNT with water, the dry SWNT sample was first exposed to saturated vapor from a water bath (1:1 weight ratio) at 110 °C for 2 h in an enclosed environment. The excess water adsorbed in the exterior of the nanotubes was then evaporated at 45 °C. An optimal filling, in terms of the H₂O/SWNT mass ratio, was found to be 11.3%. Samples of higher ratios would contain adsorbed water on the surfaces and pores outside of the nanotubes.

ND at 10 K confirmed the absence of crystalline bulk ice in SWNT + D₂O. To examine the location of the water, we concentrated on the diffraction patterns at 278 K around the first Bragg peak of SWNT at $Q = 0.4 \text{ \AA}^{-1}$ ($Q = 4\pi \sin\theta/\lambda$, where λ is the neutron wavelength) of the dry SWNT and SWNT filled with ~ 10 wt % water of three different isotopic compositions: H₂O, H₂O:D₂O = 1:1 mixture, and D₂O [Fig. 1(b)]. An ND profile can be represented as a product of the form factor $f(Q)$ and the structure factor $S(Q)$ plus an incoherent-scattering background. Here, $S(Q)$ consists of a Bragg reflection at 0.41 \AA^{-1} from the (01) planes of the two-dimensional hexagonal lattice of SWNT crystalline bundles, and $f(Q)$ of SWNT and water can be accurately calculated [17] based on the known mean dimensions of the SWNT and assumed location and composition of the H₂O/D₂O molecules. The $f(Q)$ for dry SWNT shows a minimum at 0.385 \AA^{-1} . Water residing only *inside* the nanotubes gives rise to an $f(Q)$ with a minimum at 0.385, 0.4, and 0.41 \AA^{-1} for SWNT containing H₂O, isotopic mixture, and D₂O, respectively, as shown in Fig. 1(b). Therefore, we expect an ND profile for dry SWNT and SWNT with H₂O to display a peak at $\sim 0.41 \text{ \AA}^{-1}$, whereas, for SWNT with isotopic mixture and SWNT with D₂O, this peak intensity would progressively decrease as its position

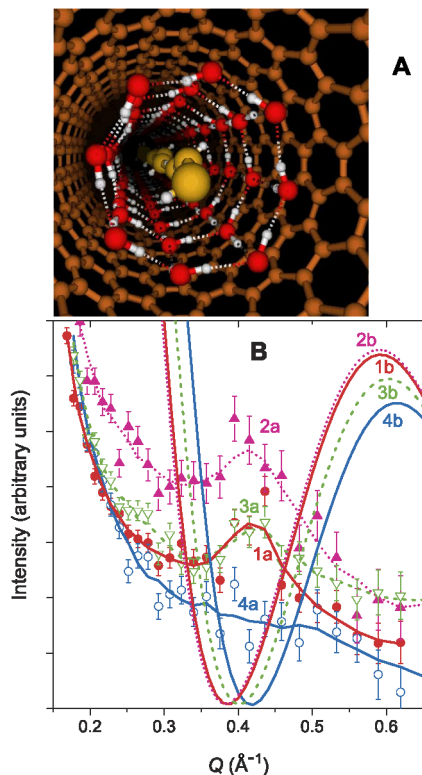


FIG. 1 (color). (a) Proposed structure of nanotube water. The interior “chain” water molecules have been colored yellow to distinguish them from the exterior “shell” water molecules (colored red). (b) Low- Q ND profiles around 0.4 \AA^{-1} for the following: 1a, dry SWNT (red curve with solid circles) and SWNT with the encapsulated water of different isotopic compositions; 2a, H_2O (pink dotted curve with solid triangles); 3a, $\text{H}_2\text{O}:\text{D}_2\text{O} = 1:1$ mixture (green short-dashed curve with open triangles); 4a, D_2O (blue solid curve with open circles). The calculated form factors for 1a, 2a, 3a, and 4a are shown by the curves labeled 1b, 2b, 3b, and 4b, respectively.

coincides with the form factor minimum. This was indeed observed as shown in Fig. 1(b). On the other hand, if water is located in the exterior region of the nanotubes, $f(Q)$ would produce minima at 0.385 , 0.38 , and 0.37 \AA^{-1} , respectively, for SWNT containing H_2O , isotopic mixture, and D_2O and therefore would give rise to ND profiles with a peak at $\sim 0.41 \text{ \AA}^{-1}$ for all samples, which is contrary to the observation.

MD simulations began with a series of slow annealing of the nanotube-plus-water system at various water densities to identify candidate structures with the lowest energy. The resultant structure showed that most of the molecules preferred to freeze along the interior of the nanotube wall in a fourfold coordinated “square-ice” pattern. Next, we investigated whether it was energetically feasible to add additional water molecules inside of the square-ice shell. Using gradient optimizations, we found that energy perturbation for adding up to 14 additional water molecules per 40 \AA of the nanotube in the form of a connected “water chain” was insignificant (0.4 out of -18.5 kcal/mol) as compared to the uncertainty of

the simulation. Figure 1(a) depicts the “shell-chain” structure of nanotube water obtained in MD simulations. Direct measurements of the short-to-intermediate range structure of the water molecules by diffraction methods are complicated by the very small changes in the peak profiles of water amid the large background from the nanotubes. In a previous x-ray diffraction study, although Maniwa *et al.* [18] found a nanotube-water structure nearly identical to that proposed by Koga *et al.* [3–5] (shell only), the authors admitted that their samples contained a substantial amount of bulk water (see, for example, Fig. 4 in Ref. [18]). This mixed location of the water might have interfered with the interpretation of the diffraction data. Our approach is to investigate the dynamics of the nanotube water by a combined INS and MD study because the vibrational spectrum of water is intense and highly sensitive to subtle structural modifications.

The INS data were collected over a wide range of wave vectors Q . The data obtained at small Q values from high incident neutron energies were crucial to the measurements of the vibrational spectra due to the extraordinarily large mean-square displacement of hydrogen, $\langle u_{\text{H}}^2 \rangle$, which severely damps the intensity with increasing Q according to $\sim \exp(-\langle u_{\text{H}}^2 \rangle Q^2)$. The measurements were made on 11.3 wt % water in SWNT, and, in addition, on a dry SWNT sample for background removal and on a bulk ice *Ih* for comparison. Figures 2(a) and 2(b) show the observed vibrational density of states (DOS) of nanotube ice at 9 K as compared with those of ice *Ih*. In general, the spectra of ice [19–25] are dominated by low-frequency intermolecular motion (e.g., translational and librational vibrations of water molecules at 0–40 and 55–120 meV, respectively) and high-frequency intramolecular vibrations (e.g., H-O-H bending around 200 meV and O-H stretching modes near 420 meV). First, the observed stretching mode frequency of nanotube ice (422 meV) is higher than that of ice *Ih* (406 meV) [Fig. 2(a)], which is in good agreement with the MD results of Martí and Gordillo [10,11]. The higher O-H stretching frequency arises from the shorter O-H covalent bonds, $R_{\text{O-H}}$, and a longer intermolecular O-O distance, $R_{\text{O-O}}$. The estimated $R_{\text{O-O}}$ of 2.916 \AA for nanotube ice at 9 K based on the observed O-H stretching frequency and a phenomenological model [26] agrees reasonably well with that ($\sim 2.81 \text{ \AA}$) predicted by our MD simulations. Comparing with the $R_{\text{O-O}}$ (2.76 \AA) of ice *Ih*, the structure of nanotube ice supports a weaker hydrogen-bonded network.

Second, the bending mode of nanotube ice consists of a narrow peak at 205 meV and a shoulder at $\sim 176 \text{ meV}$. The latter can be accounted for as the second-order overtone of the librational modes. Thus the peak at 205 meV could be assigned solely to the intramolecular H-O-H bending mode. This value is slightly larger than that for ice *Ih* ($\sim 199 \text{ meV}$).

Third, distinct features reflecting the soft hydrogen-bond dynamics unique to nanotube ice are revealed in the intermolecular motion [Fig. 2(b)]. The librational band

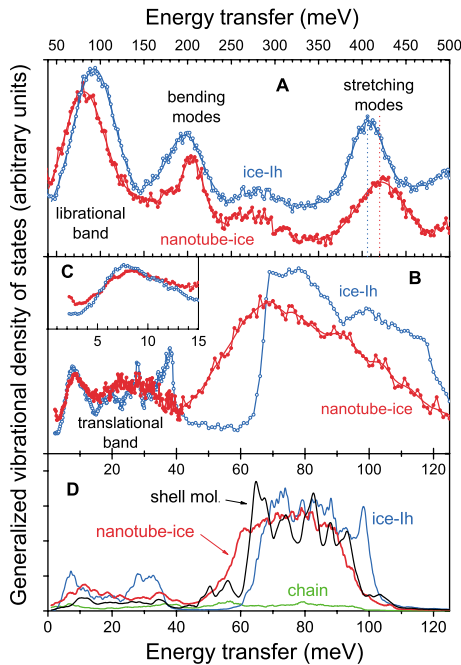


FIG. 2 (color). Experimental generalized vibrational DOS, $G(E)$, of nanotube ice and ice *Ih* at 9 K for (a) intramolecular bending (H-O-H) and stretching (O-H) modes and (b) intermolecular vibrations. A part of the observed density around 120 meV is due to multiphonon neutron scattering. The excess density below 5 meV in nanotube ice can be seen more clearly in the inset (c). (d) The $G(E)$ obtained from MD simulations at 50 K for nanotube ice, chain molecules in nanotube ice, shell molecules separately, and for ice *Ih*.

shifts to lower energies in comparison to ice *Ih*. The spectral density on the low-energy side broadens and merges with the translational band below 40 meV, which is in sharp contrast to the abrupt cutoff at ~ 67 meV in ice *Ih*. The half maximum of this band at the low-energy side occurs at 55 meV. The translational band over the 25–40 meV region broadens and lacks the salient feature that was observed for ice *Ih*. In nanotube ice the intensity of the high-energy translationlike optical modes (at ~ 36 meV) drops drastically and redistributes to lower frequencies (between 12–25 meV). Moreover, a large excess intensity appears below 5 meV [see Fig. 2(c)]. The MD simulations of a 40 Å long SWNT integrating 112 water molecules in the square-ice cylindrical shell and 14 molecules in the interior chain with respect to the simulated ice-*Ih* spectra [Fig. 2(d)] reproduce all the aforementioned structures observed in the INS experiment. Moreover, to test the structural sensitivity of the MD spectra, we simulated the cases of SWNT containing solely the square-ice shell *or* the water chain, as well as a 128-molecular assembly of proton-disordered ice *Ih*. None of these spectra showed a close resemblance to the observed data. The fact that only the interacting shell-chain structure contributes sufficient vibrational density in the 45–60 meV region and a large increase below ~ 5 meV to account for the observed spectra

lends further credence to our model of nanotube water. The excess density below 5 meV is expected to play the important role of the soft dynamics in the thermodynamics (e.g., heat capacity) and mobility of confined water.

Finally, the “softness” of nanotube water was characterized by high-resolution ($\Delta E = 80 \mu\text{eV}$) INS measurements of the $\langle u_{\text{H}}^2 \rangle$. The integrated intensity of the elastic peak $I(Q)$ was recorded over a wide range of Q at select temperatures as the sample was warmed up from 8 to 300 K. Since the signals arise predominantly from incoherent neutron scattering of hydrogen atoms, the elastic intensity follows the expression of $\ln[I(Q)] = -\langle u_{\text{H}}^2 \rangle Q^2$. In the case of bulk water [Fig. 3(b)], $\langle u_{\text{H}}^2 \rangle$ increases steadily with increasing temperature until it reaches 273 K where an abrupt increase occurs due to the melting of ice *Ih*. The data of bulk ice can be adequately explained by a harmonic potential corresponding to the measured generalized vibrational DOS [see Fig. 3(b)]. The situation for nanotube water is drastically different. The magnitude of $\langle u_{\text{H}}^2 \rangle$ for nanotube water is about 4 times larger than that for ice *Ih* throughout the 8–273 K temperature range. Note that at 8 K $\langle u_{\text{H}}^2 \rangle$ of nanotube water is already larger than the value for ice *Ih* just prior to melting. At low temperatures the absence of a quasielastic component implies solidlike behavior of nanotube water, whereas at 300 K the very large value of $\langle u_{\text{H}}^2 \rangle$ ($\sim 0.17 \text{ \AA}^2$) and observed substantial quasielastic scattering would definitely correspond to a liquidlike motion; however, there is no abrupt jump in the $\langle u_{\text{H}}^2 \rangle$ for nanotube water that resembles a solid-liquid transition of bulk water. Therefore, it is evident that on heating, the nanotube water exhibits a continuous transition from a solid to a liquid state.

The data imply a strongly anharmonic potential for nanotube water. Qualitatively, the data favor a flattened-bottom or low-barrier double-well potential with hydrogen delocalized over $\sim 0.2 \text{ \AA}$ distance, as schematically shown in the inset of Fig. 3(c). Such an anharmonic potential can qualitatively account for the observed $\langle u_{\text{H}}^2 \rangle$ up to about 120 K. At higher temperatures, additional fluctuations in terms of hydrogen-bond-breaking diffusion processes have to be included in order to explain the sharp rise of the curve. The MD result, in terms of the free energy of water molecules in a cross section of the tube, as shown in Fig. 3(a), is more revealing. At low densities the water molecules begin to fill the minimum of the LJ well. With increasing density the waters first adhere to the inside of the nanotube wall, which acts to lower the energy barrier along the center of the nanotube, eventually allowing water to occupy the interior region. The interior well is found to be much flatter and more anharmonic than the outer groove and is large enough to allow fairly easy passage of the interior molecules through the nanotube. At 50 and 100 K the chain molecules fluctuate between the local minima resembling a double-well potential. At elevated temperatures thermal activation leads to the flattening of the well and hence an additional increase of mobility. Figure 3(d) shows that the large

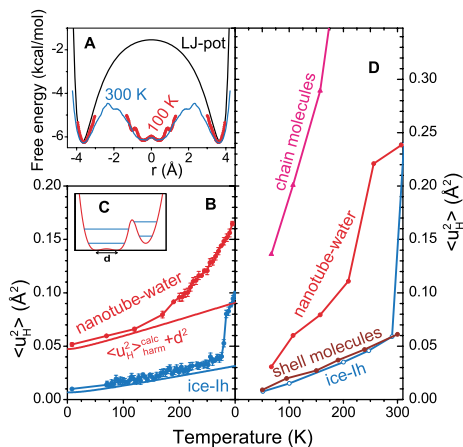


FIG. 3 (color). (a) Free energies across the nanotube walls for water molecules in nanotube water/ice at 100 (red) and 300 K (blue). The LJ potential (black) provides the minima for location of individual water molecules initially entering the SWNT. (b) Temperature dependence of $\langle u_H^2 \rangle$ in nanotube water (red circles) and in ice Ih (blue circles). The blue line shows the calculated $\langle u_H^2 \rangle$ for ice Ih according to the measured one-phonon DOS with harmonic approximation. Adding a “delocalization” of $d \sim 0.2 \text{ \AA}$ for the hydrogen atoms to the calculated curve produced the red line that matches the $\langle u_H^2 \rangle$ for nanotube water up to about 120 K. This observation suggests schematically a flattened-bottom potential and a local minimum on the side for the water molecules in the SWNT (c). (d) $\langle u_H^2 \rangle$ calculated from MD simulations of nanotube water, chain molecules in the nanotube water, shell molecules separately (see text), and ice Ih.

and rapid rising with increasing temperature of the $\langle u_H^2 \rangle$ is mainly due to thermal fluctuations of the chain molecules along the tube’s axis (showing liquidlike behavior already at 50 K), whereas the shell molecules behave like ice Ih. Since the classical model (TTM2-F) does not take into account the zero-point-energy contribution, the MD results show a smaller $\langle u_H^2 \rangle$ than the experimental values at low temperatures, but the nonlinear rise and the lack of an abrupt jump near 300 K are in qualitative agreement with experiment.

In summary, ND and INS measurements in parallel with MD simulations clearly showed the entry of water into open-ended SWNT and identified an ice-shell plus water-chain structure. The soft dynamics of nanotube water/ice arises mainly from the drastic change in hydrogen-bond connectivity of the central water chain. An average coordination number of 1.86 was found due to continually breaking/forming of the hydrogen bonds between a water molecule with its two nearest neighbors even at $\sim 50 \text{ K}$. Anomalously enhanced thermal motions along the chain direction, interpreted by a low-barrier, flattened, highly anharmonic potential well, explain the large $\langle u_H^2 \rangle$ and fluidlike behavior of nanotube water at temperatures far below the nominal freezing point. This behavior agrees qualitatively with the expected water and

proton transport via the nominally hydrophobic inner region of transmembrane proteins such as aquaporin, gramicidin, and bacteriorhodopsin [27–29].

The work performed at the Intense Pulsed Neutron Source was supported by the Office of Basic Energy Sciences, Division of Materials Sciences, U.S. Department of Energy, under Contract No. W-31-109-ENG-38. We thank R.W. Connatser and D.G. Wozniak for their assistance in the neutron-scattering experiments and A. Souza for the Raman characterization of the SWNT sample.

*Present address: Laboratoire Léon Brillouin, CEA Saclay, 91191 Gif-sur-Yvette Cedex, France.

- [1] S. Iijima, *Nature (London)* **354**, 56 (1991).
- [2] M. S. Dresselhaus, G. Dresselhaus, and P. C. Eklund, *Sciences of Fullerenes and Carbon Nanotubes* (Academic Press, San Diego, 1996).
- [3] K. Koga *et al.*, *J. Chem. Phys.* **113**, 5037 (2000).
- [4] K. Koga *et al.*, *Nature (London)* **412**, 802 (2001).
- [5] K. Koga *et al.*, *Physica (Amsterdam)* **A314**, 462 (2002).
- [6] G. Hummer, J. C. Rasaiah, and J. P. Noworyta, *Nature (London)* **414**, 188 (2001).
- [7] W. H. Noon *et al.*, *Chem. Phys. Lett.* **355**, 445 (2002).
- [8] R. J. Mashl *et al.*, *Nano Lett.* **3**, 589 (2003).
- [9] J. Wang *et al.*, *Phys. Chem. Chem. Phys.* **6**, 829 (2004).
- [10] J. Martí and M. C. Gordillo, *Phys. Rev. B* **63**, 165430 (2001).
- [11] J. Martí and M. C. Gordillo, *Phys. Rev. E* **64**, 021504 (2001).
- [12] D. J. Mann and M. D. Halls, *Phys. Rev. Lett.* **90**, 195503 (2003).
- [13] J. H. Walther *et al.*, *J. Phys. Chem. B* **105**, 9980 (2001).
- [14] C. J. Burnham and S. S. Xantheas, *J. Chem. Phys.* **116**, 1500 (2002).
- [15] C. J. Burnham and S. S. Xantheas, *J. Chem. Phys.* **116**, 5115 (2002).
- [16] I. W. Chiang *et al.*, *J. Phys. Chem. B* **105**, 8297 (2001).
- [17] S. Kline and A. Munter, *Model CoreShellCylinder* <http://www.ncnr.nist.gov/resources/sansmodels/CoreShellCylinder.html>, 1999.
- [18] Y. Maniwa *et al.*, *J. Phys. Soc. Jpn.* **71**, 2863 (2002).
- [19] A. I. Kolesnikov *et al.*, *Phys. Lett. A* **168**, 308 (1992).
- [20] J. Li, *J. Chem. Phys.* **105**, 6733 (1996).
- [21] H. Schober *et al.*, *Physica (Amsterdam)* **241B**, 897 (1997).
- [22] A. I. Kolesnikov *et al.*, *Phys. Rev. B* **59**, 3569 (1999).
- [23] J. C. Li *et al.*, *Phys. Rev. B* **59**, 9088 (1999).
- [24] J. S. Tse *et al.*, *Nature (London)* **400**, 647 (1999).
- [25] J. S. Tse *et al.*, *Phys. Rev. Lett.* **85**, 3185 (2000).
- [26] D. D. Klug and E. Whalley, *J. Chem. Phys.* **81**, 1220 (1984).
- [27] Y. Kong and J. Ma, *Proc. Natl. Acad. Sci. U.S.A.* **98**, 14345 (2001).
- [28] R. Pomes and B. Roux, *Biophys. J.* **82**, 2304 (2002).
- [29] J. K. Lanyi, *J. Phys. Chem. B* **104**, 11441 (2000).